Study of Tin-Silver Solder Ball Bump Bonded Hybrid Silicon Pixel Detector

S. Arab[1], *S. Choudhury*[1], *G. Dolinska*[1], *E. Garutti*[2], *K. Hansen*[1], *M. Hoffmann*[2], *I. Korol*[1], *H. Perrey*[1], *D. Pitzl*[1], *J. Pöhlsen*[2], *V. Sola*[2], *S. Spannagel*[1], *G. Steinbrück*[2]

[1]Deutsches Elektronen-Synchrotron DESY - Hamburg, Germany
[2]University of Hamburg, Germany

DOI: http://dx.doi.org/10.3204/DESY-PROC-2014-04/45

For the connection of front-end readout chips to a silicon sensor of a hybrid pixel detector an in-house flip-chip bump bonding process using precision tin-silver solder balls has been implemented at DESY. The electrical testing of the bump connections follows immediately using an automated probe station by sensing a capacitively induced charge. The bump bonding quality and results from thermal stress testing has been reported. The pixel detector modules have been evaluated in the DESY electron test beam in terms of tracking efficiency and position resolution which has been summarized.

1 Introduction

The process of bump bonding of the silicon sensor to the front-end readout electronics is defining step in the fabrication of a hybrid pixel detector and the procedure of pixel detector module production at DESY with bump bonding of the front-end readout chip to the silicon sensor and quality tests of the bump bond by electrical method and radioactive source have been outlined. The module has also been tested in the electron beam at DESY in terms of charge collection, noise, tracking efficiency and position resolution. The PSI designed and IBM fabricated front-end readout chip [1] measuring 150 x 100 μm^2 has been used to establish the process of high precision tin-silver solder ball bump bonding at DESY to the silicon sensor [2] fabricated from 285 μm thick silicon. The pixels are arranged in an array of 52 columns and 80 rows in a single read-out chip with a double column readout structure for data and time stamp buffers. The new readout chip is an evolution of the one used for the present detector with lower charge thresholds and increased readout link speeds with higher time stamp and data buffer sizes and Fast Input Fast Output (FIFO) buffer. The sensor technology remains the same with n$^+$ in n substrate as the collection of electrons is advantageous because of their higher mobility compared to holes, which causes a larger Lorentz drift of the signal charges. This drift leads to charge sharing between neighbouring pixels and thus improves the spatial resolution. Furthermore, the higher mobility of electrons makes them less prone to trapping, which leads to a higher signal charge after high fluences of charged particles. After irradiation induced space charge sign inversion, the highest electric field in the sensor is located close to the n$^+$ electrodes used to collect the charge, which is also an advantage. The choice of n-substrate requires a double sided sensor process, meaning that both sides of the sensor need photo-lithographic processing. The double sided sensors have a guard ring scheme where all sensor edges are at a ground potential, which greatly simplifies the design of detector modules which ensures a high signal charge at moderate bias voltages ($\leq$ 600 V) after high hadron fluences. The n-side isolation is implemented through a moderated p-spray technique with a punch through biasing grid. The sensor wafer sample in this study has been obtained from PSI which were processed on approximately 285 μm thick n-doped diffusion oxygenated float zone silicon.

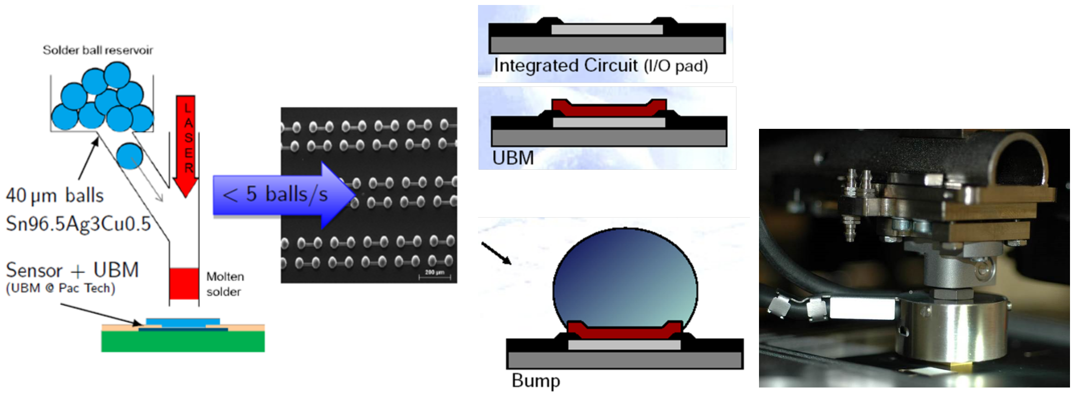

Figure 1: The bump bonding process with the solder ball deposition from SB^2 laser jetting system and the Femto flip-chip bonder for the connection of the sensor and readout chip.

2 Sn-Ag Solder Ball Bump Bonding at DESY

The bump bonding process remains a crucial and the most expensive step towards production of a silicon pixel detecor module and this process has been assembled at DESY with a SB^2 laser jetting system [3] and flip chip bonder [4] to make high precision tin-silver solder ball connections of the readout chip to the silicon sensor.

2.1 Bump Bonding Technique

The bump bonding process can be divided into 3 steps: under-bump metal (UBM) composed of Ni-Pd-Au deposition, solder sphere deposition, and flip chip bonding with re-flow soldering followed by the bare module electrical tests. This is done using an SB^2 step motor controlled bump deposition machine from PacTech. Solder balls of 40 μm diameter with a composition of 96.5% Sn, 3% Ag and 0.5% Cu are dropped though a capillary, molten by a laser and then placed onto the bump pad of the sensors where they solidify. The step-motor places the solder balls with a rate just below 5 Hz, which results in approximately 5 h bump deposition time per sensor with a 16-chip assembly. The next step is the bonding of the sensor onto the read-out chip using a Finetech Femto flip-chip bonder, to form the mechanical and electrical connection. The electronics wafers are thinned by back grinding and the sensor and electronics wafer are cut to get the sensor tiles and the front-end chips. The readout chip is aligned on the sensor tile in such a way that the front-end bumps face the relative sensor bump pads. The tuning of the process parameters has been performed using glass substrates in order to better investigate the effects on bumps by simple inspection under microscope. The chosen mating pressure is 160 N/chip, applied on the wafers heated around the melting point of tin at 240°C in a formic acid atmosphere. The resulting bump height after the flip-chip bonding process is 26 μm (reduced from 40 μm diameter solder ball).

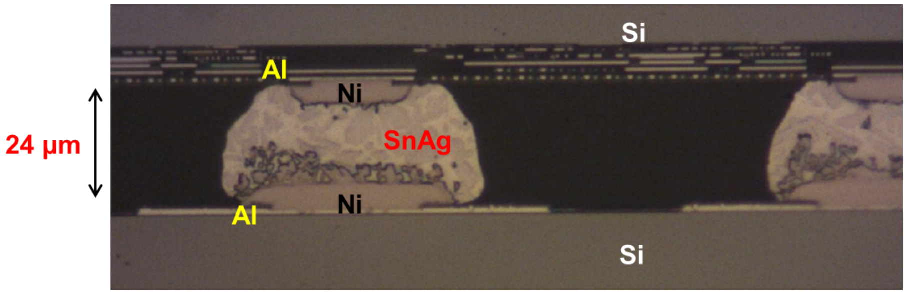

Figure 2: The side view of the bump bonds with the nodule cut across vertically and polished to examine under microscope.

2.2 Test of Bump Bonding Quality

To test that the front-end readout chip is performing as expected, scans of the analog response is carried out. The sensor is kept at a bias voltage of -100 V. A charge is injected into each pixel 10 times and the response recorded. The result should equal 10 and should have a uniform output for a perfect chip, and the result is as expected for 4160 pixels in the single chip module. This is termed as the "pixel alive test" which is to demonstrate the fully functional pixels in the module. The next step is electrical testing of the quality of the bumps and this is done by charge pulses and inducing the charge capacitively directly through the air capacitance between the readout chip and the sensor and then reading out the analog pulse height through the sensor and subsequently bump bonds. In case of missing bumps, the pulse height distribution would be at zero and if the pulse is read through good bumps, then this would be seen at positive values. The pulse height map is shown in Figure 3 with 2 missing bumps at the top left corner (row 0 col 78, row 0 col 79) and 4158 perfect bonds well separated and at positive values. This test is reconfirmed with a radioactive β-ray source. A ^{90}Sr source has been used for inducing signals in the sensor. The β-spectrum of the daughter decay of ^{90}Y has an endpoint energy of about 2.3 MeV and therefore contains particles which approximate a minimum ionising particle. From the hit map, 2 missing bonds can be seen at the top left edge of the module thereby confirming the validity of the electrical testing.
The module is then subjected to several thermal stress cycles from temperature -17°C to +25°C back and forth over a span of one week. The bump bonding test is performed before the start of the the thermal stress cycle and then at the end of each high and low temperature cycle and finally at the end of the cycle, and all tests show the same result as had been obtained previously in Figure 3 showing that the connections are intact and no dislocation of the bumps have taken place due to the thermal stress. The thermal stress cycle establishes the strenghth of the solder ball bump connections and its ability to withstand temperature fluctuations.

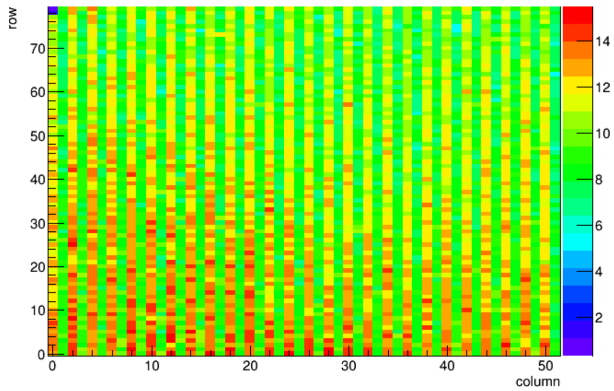

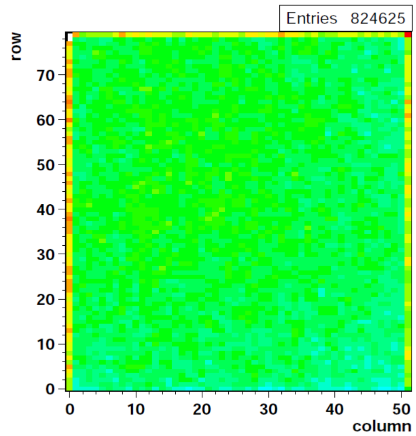

Figure 3: The pulse height map for bump bonding test from capacitively induced charge across the sensor through the air gap capacitor between readout chip and sensor (on left) and the hit map from a β-ray ^{90}Sr source for confirmation of the bump bonding electrical test (on right).

3 Beam Test Studies in DESY Electron Beam

New detectors are required to be tested in an environment similar to that in which they will be exposed in order to determine the performance. A beam test, where the device is read out within a beam of particles, is preferable to using a radioactive source in a laboratory since the statistics will be much higher. The particle type and energy is usually well known within a beam test, however the exact position of a particle at any given time is difficult to determine. Therefore, a set of well understood detectors known as a telescope is used in beam test experiments to track the charged particles. These tracks can be reconstructed offline to evaluate the efficiency and charge sharing performance of the devices under test for various parameters such as the tilt angle, threshold or bias voltage.

3.1 Test Beam Experimental Setup at DESY

The data studied in this analysis was taken at the DESY electron beam with the EUDET pixel telescope having 6 planes of Mimosa 26 sensor developed for ILC [5] with the pixel device under test midway and a reference pixel for timing reference mounted at the end of the beam line. The DESY synchrotron accelerates electrons and then a carbon fibre placed in the beam line produces photons through bremsstrahlung radiation. These photons impact a metal plate which converts them to pairs of electron and positron. A dipole magnet spreads the beam out as a function of the sign and energy. The desired beam energy within the range of 1-6 GeV is chosen with a collimator. The beam line has been configured to provide 5.2 to 5.6 GeV electrons. The beam size is approximately 3 cm (FWHM) and the beam intensity has been tuned to 1 kHz/cm^2. The EUDET telescope [6, 7] consists of two arms each equipped with three sensors. The positions of the sensors along the beam axis can be adapted to the respective requirements. Between the two arms optional mechanical x-y support stage that allows to position the Pixel Device Under Test (DUT) and Reference Pixel (REF) with a few micron precision is installed. Since the telescope is read out at a rate of 112 μs in a rolling shutter mode and the DUTs are read out every 400 ns, the reference sensor is primarily there to

determine if a hit on the DUT is registered thus serving as a timing reference. The sensors are read out by dedicated data-reduction boards that transfer their data to a computer where the data acquisition software is running. A trigger system including four scintillators connected to photomultiplier tubes allows to trigger on particles passing the telescope. For this, two pairs of scintillators (1x2 cm^2), each pair perpendicular to each other, are located in coincidence either side of the telescope to trigger on the incident particles.
The Mimosa sensors typically provide a signal-to-noise ratio for minimum ionising particles (MIPs) of 20-40 and a detection efficiency for MIPs of $> 99\%$ depending on the thresholds. The Mimosa 26 sensor is a combination of the Mimosa 22 sensor [8] and the SuZe01 chip [9] that performs online data sparsification. The sensor is subdivided into 1152 columns of 576 pixels with a pitch of 18.4 μm providing a high granularity. The sensitive area of the sensors is approximately 21 x 10.6 mm^2. On each pixel an amplification and CDS circuit is implemented. The sensor is read out in a column-parallel mode with a pixel-readout frequency of 80 MHz which results in a integration time of about 112 μs. Each column is equipped with a discriminator that performs an offset compensation and a second column double sampling.

3.2 Readout Chip Characterization and Data Acquisition

A threshold setting is required for the front-end card to limit the noise recorded from the module. The output from a threshold scan for the pixel device is tuned to 3100 electrons which is important for charge sharing and influences position resolution and efficiency after irradiation. The measured noise is 160 electrons obtained from the width of the threshold curve. There is a higher level of noise for a lower threshold tuning. The noise for the SnAg bump bonded pixel modules at DESY is similar to Indium bump bonded pixel modules at PSI with the same readout chip.
The data acquisition system is the one for EUDET pixel telescope with a flexible data acquisition software (EUDAQ) [10, 11, 12] for testing the pixel module with the MIMOSA sensors of the telescope system for track interpolation and extrapolation to the DUT. The hardware of the telescope and of the connected DUTs is read out by separate producer tasks that are connected to the “run control” and the “data collector”. The latter receives the data streams, builds the events and stores the data on the storage device. The “log collector” provides an interface for the producers for the collection of logging messages. One part of the EUDAQ software is the online-monitoring system (RootMonitor) that makes use of the object-oriented data analysis framework ROOT [13] implemented in C++. The RootMonitor can be used together with the EUDAQ system during data taking as well as a stand-alone application reading and analysing raw data files. The RootMonitor is able to handle different sensor types for the various telescope planes. It provides a simple fixed-frame cluster reconstruction algorithm. Seed pixel candidates are identified and starting from the pixel with the highest signal-to-noise ratio clusters are constructed by joining neighbouring pixel to the cluster if certain thresholds are fulfilled. Thus it starts from one hit candidate and then assigns all 8 neighbouring hit pixels to the cluster. This procedure is repeated until all hit pixel are joined into clusters. The cluster position is reconstructed in the RootMonitor by determining the centre-of-gravity for each cluster which is a signal-weighted average of the pixel positions belonging to the cluster.

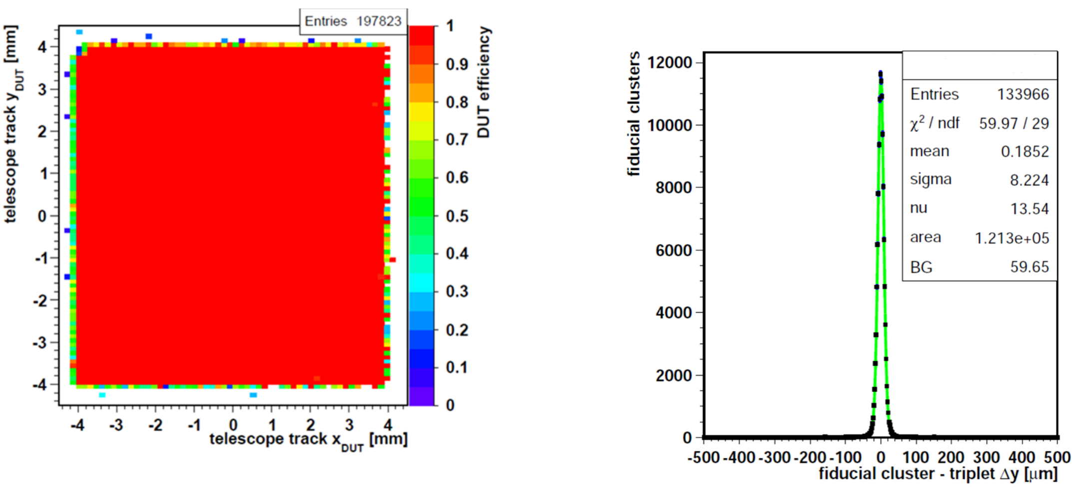

Figure 4: The map of tracking efficiency in a single-chip module (on left) and the position resolution with a fit to Gaussian (on right).

3.3 Test Beam Measurements and Data Analysis

The offline analysis software (EUTelescope) [14, 15] for the telescope data is based on Marlin [16, 17, 18] and Linear Collider In / Out (LCIO) [19, 20]. The EUTelescope software makes use of the Marlin analysis framework which divides the analysis in several individual small tasks. The behaviour of these processors can be controlled with steering files. The data is stored in the LCIO format which was developed to provide a persistent data model and interface. The pedestal and noise information are determined and hit pixels are grouped into clusters by applying a loose selection and quality criteria. The cluster coordinates are transformed from the local reference frame to the global telescope reference frame using the geometry description provided by the GEAR [21] package. After determining the alignment constants of the individual planes, the fitter reconstructs tracks using this collection of corrected hits. These tracks can be used for an extrapolation to the DUT surface in order to determine the predicted positions of hits in the DUT plane. For all hit pixels the number of neighbouring hit pixels is determined, whereas diagonal neighbours are ignored. The list of hit pixels obtained in the previous step is sorted with decreasing neighbours in order to determine the seed candidates. For pairs of pixel with equal number of neighbours, the pixel with the larger number of diagonal neighbours is preferred. The resulting list is processed starting from the seed candidate with the highest number of neighbours. All hit pixels in a fixed x-y frame around the seed pixel are merged into the cluster and removed from the pixel collection and from the list of seed candidates.
In order to be able to reconstruct tracks with the telescope and to extrapolate these tracks to the DUT plane, the geometrical positions of the sensor planes have to be known with high precision. Beam particles passing the telescope planes create clusters in the sensors which are spatially correlated between the individual planes. The EUTelescope software packages provides a processor (EuTelMille) that uses MILLEPEDE [22, 23] for the determination of the alignment constants in order to reduce the bias and the uncertainty of the fitted track parameters and to minimize the χ^2 of the tracks. Each parametrisation of a track depends on local parameters that vary between the tracks and on global parameters - the alignment constants. The processor

EuTelMille takes as an input a collection of hits and then for all combination of hits straight lines are fitted to these groups of hits independently in x and y direction. In order to suppress fake tracks resulting from combinatoric background, cuts on the residual distributions for all sensor planes can be specified in the corresponding steering file. The derivatives of the tracks with respect to all local and global parameters are stored in a binary file that can be read by Millepede. The Millepede software determines in a simultaneous linear least-squares fit of all local and global track parameters the alignment constants for the sensor planes.
Charge sharing improves track position resolution, but charge that is shared between two (or more) neighbouring pixels reduces the charge each pixels receives. This increases the likelihood that the charge per pixel is below threshold, but this is done away with a low charge threshold. Charge sharing will increase when the sensor is tilted, since particle tracks will pass through multiple pixels. The coordinate measured by a pixel detector is obtained by the position of the centre of the cluster of hit pixels associated with a track, plus a correction (conventionally called the η function) which is a function of the charge sharing, the cluster width and the track angle. The position resolution is calculated by comparing the track position interpolated by the telescope planes and the pixel hit position calculated using charge sharing between rows. The difference of this distribution which is termed as the residual is fitted to a Gaussian. The residuals are calculated separately for x and y and are the difference between the position of the reconstructed track and the position of the cluster centre. The Gaussian shape is due to charge sharing at the edge of the pixels and is wider with increase in multiple scattering. The best position resolution of 7.0 μm for the lower threshold of 1.8 ke is reached at the angle where optimal charge sharing between neighboring pixels occurs, that is where the particles most likely traverse two pixel cells. This optimal angle is determined by the pixel geometry from inverse tangent of the ratio of pixel width in row direction to sensor thickness and is 19.3° along the row direction in which the pixels have a width of 100 μm and the sensor thickness being 285 μm. The position resolution of 7.0 μm is obtained from the residual width 8.2 μm in Figure 4, correcting for the telescope resolution of 4.3 μm.
The tracking efficiency for a pixel sensor is defined as the ratio of the number of measured hits close to a track, against the total hits predicted. These expected hits are determined using reconstructed tracks from the beam test. The tracks are extrapolated from the telescope hits to the DUT plane. To reduce fake tracks, a matching hit in the reference sensor is required. The tracking efficiency is thus defined as the ratio of the DUT hit linked to isolated telescope track with link to REF hit to all the isolated telescope tracks with link to REF hit. The isolation in the telescope track is required due to pileup in the telescope (3-5 tracks/event) which leads to confusion and random overlays at the REF plane. With the module tilted at 19.3°, the efficiency is 99.96% in the fiducial region as observed in Figure 4 and is also observed to remain constant with time. Finally, the test beam profile at vertical tracking incidence in Figure 5 reaffirms the electrical bump bonding test in the laboratory with the observed 2 missing bump connections.

4 Conclusion

The procedure for Femto flip-chip bump bonding with a SB^2-Jet (Laser Solder Jetting System) using high pecision Sn-Ag solder balls to connect the read-out chip to the silicon sensor has been successfully implemented at DESY for production of a hybrid silicon pixel detector. The SB^2 solder ball jetter places the Sn-Ag bumps at a rate of 4.5 Hz and then a flip chip bonder makes

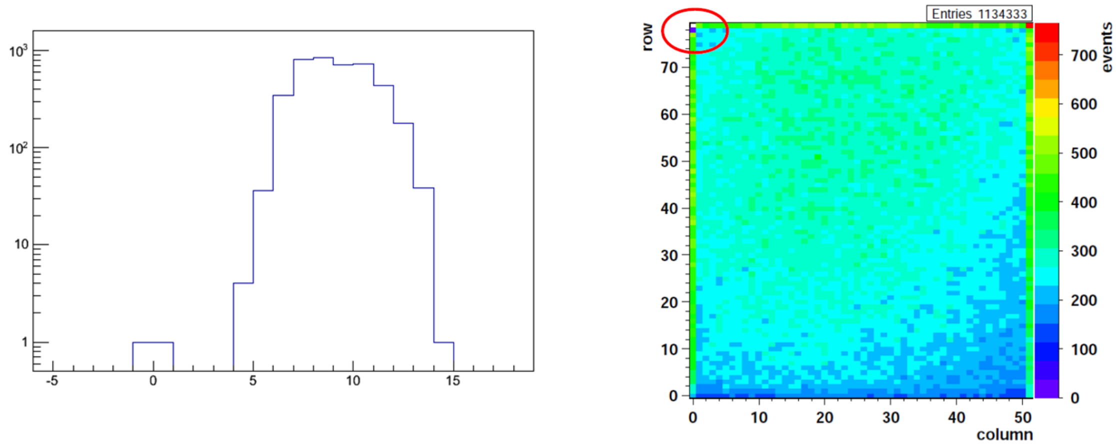

Figure 5: The pulse height distribution from capacitively induced charge across the sensor through the air gap capacitor between readout chip and sensor showing bump bonding test (on left) and the test beam profile shown at vertical incidence to reaffirm the bump bonding electrical test (on right).

the connection at 240°C with 160 N tacking force with re-flow in a formic acid atmosphere. The quality for the bump bonding has been tested electrically and with radioactive source in the laboratory and using the electron test beam at DESY and subsequently through several thermal stress cycles and the module quality is found to be excellent. The position resolution of the module is 7.0 μm with a tracking efficiency of up to 99.96% in the fiducial region for the optimum charge sharing tilt angle between pixels. In a similar way other high quality modules have been produced and tested at DESY successfully preparing the laboratory for the production of a silicon pixel detector.

Acknowledgments

The authors would like to thank the pixel detector group of Roland Horisberger at PSI for the front-end readout chip and sensor used for this study and the DESY accelerator personnel for the smooth and steady delivery of the test beam during the data taking periods.

References

[1] H. Chr. Kaestli et. al., "Design and performance of the CMS pixel detector readout chip", Nucl. Instr. Meth. A 565, 188 (2006).

[2] T. Rohe et. al., "Planar sensors for the upgrade of the CMS pixel detector", Nucl. Instr. Meth. A 650, 136 (2011).

[3] PacTech - Solder Jetting & Solder Deballing and Reballing, URL $http://www.pactech.com/index.php?option = com\_content\&view = article\&id = 16\&Itemid = 6$.

[4] FineTech - Femto Flip-Chip Bonder, URL $http://eu.finetech.de/products/micro - assembly/fineplacerr - femto.html$.

[5] J. Brau, Y. Okada and N. Walker (Ed.) et. al., "ILC Reference Design Report Volume 1 - Executive Summary", arXiv:0712.1950 [physics.acc-ph].

[6] D. Haas, "The EUDET High Resolution Pixel Telescope - Towards the Final Telescope", EUDET-Report-2008-02, 2008.

[7] L. Reuen and J. Furletova, "JRA1 - The DEPFET sensor as the first fully integrated DUT in the EUDET pixel telescope: The SPS test beam 2008", EUDET-Memo-2008-34, 2008.

[8] G. Claus et. al., "JRA1 Milestone IDC Prototype ready", EUDET-Memo-2008-03, 2008.

[9] A. Himmi et. al., "A Zero Suppression Micro-Circuit for Binary Readout CMOS Monolithic Sensors", Proceedings of TWEPP-09: Topical Workshop on Electronics for Particle Physics, Paris (France), pg. 426-430, 2009.

[10] M. Pohl, D. Haas and E. Corrin, "JRA1 - Data acquisition system", EUDET-Memo-2006-07, 2006.

[11] D. Haas, "The DAQ for the EUDET pixel telescope", Proceedings of 2007 International Linear Collider Workshop (LCWS07 and ILC07), Hamburg (Germany).

[12] E. Corrin, "EUDAQ Software User Manual", EUDET-Memo-2010-01, 2010.

[13] R. Brun and F. Rademakers, "ROOT: An object oriented data analysis framework", Nucl. Instr. Meth. A 389, 81 (1997).

[14] A. Bulgheroni et. al., "Eutelescope: tracking software", EUDET-Memo-2007-20, 2007.

[15] A. Bulgheroni et. al., "EuTelescope - the JRA1 tracking and reconstruction software: a status report (Milestone)", EUDET-Memo-2008-48, 2008.

[16] F. Gaede, "Marlin and LCCD: Software tools for the ILC", Nucl. Instrum. Meth. A 559, 177 (2006).

[17] "Marlin". URL $http://ilcsoft.desy.de/portal/software\_packages/$.

[18] J. Engels and F. Gaende, "Marlin - A Software Framework for ILC detector R&D", EUDET-Report-2007-11, 2007.

[19] F. Gaede et. al., "LCIO: A persistency framework for linear collider simulation studies", arXiv: physics/0306114.

[20] "LCIO", URL $http://lcio.desy.de/$.

[21] "GEAR - A geometry description toolkit for ILC reconstruction software". URL $http://ilcsoft.desy.de/portal/software\_packages/gear$.

[22] V. Blobel and C. Kleinwort, "A New Method for the High-Precision Alignment of Track Detectors", DESY-02-077 pg. 10, 2002.

[23] V. Blobel, "Millepede", URL $http://www.desy.de/\ blobel$.